

Extreme C Terminus of Bacterial Cytoskeletal Protein FtsZ Plays Fundamental Role in Assembly Independent of Modulatory Proteins^{*[5]}

Received for publication, December 3, 2011, and in revised form, January 18, 2012. Published, JBC Papers in Press, February 1, 2012, DOI 10.1074/jbc.M111.330324

Paul J. Buske and Petra Anne Levin¹

From the Department of Biology, Washington University, Saint Louis, Missouri 63130

Background: Assembly of the cytoskeletal protein FtsZ into a loose bundle of filaments at the nascent septum initiates bacterial cell division.

Results: The extreme C terminus of FtsZ mediates electrostatic interactions between FtsZ polymers.

Conclusion: The FtsZ C terminus promotes lateral interactions *in vitro* and ensures efficient division *in vivo*.

Significance: The extreme C terminus of FtsZ plays a role to promote its own stabilization.

Bacterial cell division typically requires assembly of the cytoskeletal protein FtsZ into a ring (Z-ring) at the nascent division site that serves as a foundation for assembly of the division apparatus. High resolution imaging suggests that the Z-ring consists of short, single-stranded polymers held together by lateral interactions. Several proteins implicated in stabilizing the Z-ring enhance lateral interactions between FtsZ polymers *in vitro*. Here we report that residues at the C terminus of *Bacillus subtilis* FtsZ (C-terminal variable region (CTV)) are both necessary and sufficient for stimulating lateral interactions *in vitro* in the absence of modulatory proteins. Swapping the 6-residue CTV from *B. subtilis* FtsZ with the 4-residue CTV from *Escherichia coli* FtsZ completely abolished lateral interactions between chimeric *B. subtilis* FtsZ polymers. The *E. coli* FtsZ chimera readily formed higher order structures normally seen only in the presence of molecular crowding agents. CTV-mediated lateral interactions are important for the integrity of the Z-ring because *B. subtilis* cells expressing the *B. subtilis* FtsZ chimera had a low frequency of FtsZ ring formation and a high degree of filamentation relative to wild-type cells. Site-directed mutagenesis of the *B. subtilis* CTV suggests that electrostatic forces are an important determinant of lateral interaction potential.

FtsZ is an essential cytoskeletal protein that plays a central role in bacterial cell division. Conserved in bacteria, archaea, and chloroplasts, FtsZ assembles into a ring structure at the nascent division site (the FtsZ ring) that serves as a scaffold for assembly of the division machinery (1). The FtsZ ring is dynamic, with average subunit turnover time estimated to be between 8 and 30 s (2). At the end of the cell cycle, the FtsZ ring constricts at the leading edge of the invaginating septum. Approximately 30% of total FtsZ is in the FtsZ ring, whereas the remainder appears to be largely cytoplasmic (2).

^{*} This work was supported, in whole or in part, by National Institutes of Health Public Health Service Grant GM64671 (to P. A. L.).

^[5] This article contains supplemental Tables S1 and S2, Figs. S1–S4, and References.

¹ To whom correspondence should be addressed: Dept. of Biology, Washington University, Box 1137, 1 Brookings Dr., Saint Louis, MO. Tel.: 314-935-7888; Fax: 314-943-4432; E-mail: plevin@wustl.edu.

Like its eukaryotic homolog tubulin, FtsZ binds GTP as a monomer; however, a GTPase active site is formed only after dimerization (3). *In vitro*, FtsZ assembles into single-stranded polymers, or protofilaments, in the presence of GTP (4). Increasing the concentrations of divalent cations like Mg²⁺ or Ca²⁺ or adding crowding agents, such as methyl cellulose or DEAE-dextran to purified *Escherichia coli* and *Bacillus subtilis* FtsZ stimulates lateral interactions between protofilaments, leading to the formation of bundles, spirals, tubes, and sheets (5–8).

High resolution imaging techniques suggest that *in vivo* the FtsZ ring is composed of short, single-stranded protofilaments that are linked together via lateral interactions. Cryo-EM tomography indicates that the FtsZ ring is made up of short filaments (~100 nm) concentrated at the division site (9). Photoactivated localization microscopy suggests that FtsZ protofilaments are arranged around midcell in a randomly oriented loose bundle (10). Lateral interactions are mediated in part through the actions of FtsZ modulatory proteins, including the widely conserved ZapA protein, as well as ZipA and SepF, which are limited to the γ group of Gram-negative bacteria and the Firmicutes, respectively (11).

Structural and phylogenetic analysis divides the FtsZ subunit into five domains: the unstructured and poorly conserved N terminus, the globular highly conserved core, an unstructured C-terminal linker, a short, well conserved “C-terminal tail” (CTT), and finally a small, highly variable set of residues (12–14), termed here the C-terminal variable region, or CTV (Fig. 1A). For simplicity, we have grouped the N-terminal peptide and core together. The FtsZ core displays a Rossman fold typical of nucleotide binding proteins, including the residues comprising the GTP binding site and the T7 synergy loop required for GTP hydrolysis (3). The core has been extensively studied, and a handful of residues essential to longitudinal subunit bonds at the dimer interface have been mapped to this region (15–17). Residues implicated in lateral interactions between protofilaments have also been mapped to the core (supplemental Table S1).

Following the core is the C-terminal linker. In *B. subtilis* and *E. coli*, the region spans ~50 residues but can span over 300

The C Terminus of FtsZ Mediates Lateral Interactions

residues in some bacterial species (13). The C-terminal linker is irresolvable by crystal structure, and we have modeled it here as an unstructured peptide as proposed by Erickson (3) (Fig. 1A).

The next 11 residues of FtsZ constitute the conserved CTT² (Fig. 1A). The CTT is critical for interactions between FtsZ and several modulatory proteins, a function analogous to tubulin's C-terminal tail. The stabilizing proteins FtsA and ZipA require the CTT for an interaction with FtsZ in *E. coli* (18–20). In *Caulobacter crescentus*, deletion of the CTT disrupts the FtsZ-FtsA interaction and leads to a punctate FtsZ localization pattern (21). Similarly, *E. coli* FtsZ CTT point mutants are resistant to overexpression of the division inhibitor MinC^C/MinD, and at least one CTT mutant is unable to bind MinC^C *in vitro* (22). EzrA, an inhibitor of FtsZ assembly in *B. subtilis*, disrupts assembly of full-length FtsZ but does not appear to interact with a truncated protein missing the last 16 residues, a region that includes the CTT (23).

Although the proteins that bind to it are not all conserved, the majority of CTT residues implicated in interactions with modulatory proteins are themselves conserved (Fig. 1B and supplemental Table S1). The 4 CTT residues, Asp-373, Ile-374, Phe-377, and Leu-378, implicated in interactions between FtsZ and FtsA, MinC, and ZipA, are conserved in FtsZs from a diverse array of species (Fig. 1B). This high degree of conservation suggests the CTT may play a role in FtsZ assembly beyond its function as a “landing pad.”

The residues between the CTT and the very C terminus of FtsZ are highly variable both in length and content. In *B. subtilis* FtsZ, this region is 6 residues but spans up to 10 residues in *Staphylococcus aureus* FtsZ and can be positive, negative, or neutral in charge. We have termed this region the C-terminal variable (CTV) domain.

Here we report that the *B. subtilis* CTV is both necessary and sufficient for promoting lateral interactions between FtsZ protofilaments in the absence of modulatory proteins. Comparative analyses of mutant and chimeric *B. subtilis* and *E. coli* FtsZs indicate that changes in the CTV have dramatic impacts on the bundling capacity of each protein. CTV charge appears to be the primary determinant of its potential to promote lateral interactions. Supporting a role for the CTV in mediating lateral interactions between FtsZ polymers *in vivo*, defects in the *B. subtilis* FtsZ CTV severely impair FtsZ ring formation and cell division. This work has implications for our understanding of FtsZ assembly processes as well as the role of modulatory proteins in controlling FtsZ lateral interactions.

EXPERIMENTAL PROCEDURES

General Methods and Strain Construction—All *B. subtilis* strains are derivatives of the strain JH642 (24). Cloning and genetic manipulation were performed using standard techniques (25, 26). All cloning was done using the *E. coli* strain AG1111 (27), with the exception that *B. subtilis* ftsZ vectors were cloned in the AG1111 derivative PL930. PL930 contains

² The abbreviations used are: CTT, C-terminal tail; CTV, C-terminal variable region; CTVB, C-terminal variable region from *B. subtilis*; CTVE, C-terminal variable region from *E. coli*; L/R, cell length/FtsZ ring ratio; Bs, *B. subtilis*; Ec, *E. coli*.

TABLE 1
Bacterial strains and plasmids used in this study

Strain or plasmid	Genotype and/or features	Source
<i>B. subtilis</i> strains		
JH642	<i>B. subtilis</i> trpC2 pheA1	Ref. 24
PL2084	JH642 thrC::P _{xyt} -ftsZ _{Bs} ^Δ ftsZ _{Bs} ::spc, xylA::tet	Ref. 30
PL3176	PL 2084 amyE::P _{spac} -ftsZ _{Ec}	This study
PL3178	PL 2084 amyE::P _{spac} -ftsZCTVB _{Ec}	This study
PL3188	JH642 ftsZ::ftsZ	This study
PL3189	JH642 ftsZ::ftsZCTVE _{Bs}	This study
<i>E. coli</i> strains		
MG1655	F ⁻ λ ⁻ ilvG ⁻ rfb-50 rph-1	
AG1111	DZR200- MC1061 F ⁺ lacIQ lacZM15 Tn10 (tet)	Ref. 27
C41 (DE3)	F ⁻ ompT hsdSB (rB ⁻ mB ⁻) gal dcm (DE3)	Ref. 34
PL930	AG111 + pBS58	Ref. 30
PL2452	MG1655 leu::Tn10-ftsZ84 (ts)	Laboratory stock
Plasmids		
pPJ1	pET-21b (+)-ftsZ _{Bs} stop	This study
pPJ2	pET-21b (+)-ftsZ _{Ec} stop	This study
pPJ3	pET-21b (+)-ftsZΔC17 _{Bs} stop	This study
pPJ4	pET-21b (+)-ftsZΔC15 _{Ec} stop	This study
pPJ5	pET-21b (+)-ftsZCTVE _{Bs} stop	This study
pPJ6	pET-21b (+)-ftsZCTVB _{Ec} stop	This study
pPJ7	pET-21b (+)- ftsZKNRKG _{Bs} stop	This study
pPJ8	pET-21b (+)- ftsZENDEG _{Bs} stop	This study
pPJ9	pDR67-ftsZ _{Bs} stop	This study
pPJ10	pDR67-ftsZCTVE _{Bs} stop	This study
pPJ11	pDR67-ftsZ _{Ec} stop	This study
pPJ12	pDR67-ftsZCTVB _{Ec} stop	This study
pPJ13	pJL74-ftsZ _{Bs} stop	This study
pPJ14	pJL74-ftsZCTVE _{Bs} stop	This study

the low copy plasmid pBS58 expressing *E. coli* ftsQAZ, which facilitates cloning of *B. subtilis* FtsZ (28). Vent DNA polymerase was used for PCRs (New England Biolabs).

Cells were grown in Luria-Bertani (LB) medium at 37 °C unless otherwise noted. Antibiotics were used at the following concentrations: ampicillin = 100 μg ml⁻¹, spectinomycin = 100 μg ml⁻¹, tetracycline = 12.5 μg ml⁻¹, chloramphenicol = 5 μg ml⁻¹.

Strains and plasmids used in this study are listed in Table 1. A list of primers used with restriction sites can be found in supplemental Table S2. The plasmids pPJ1–12 were constructed first by PCR-amplifying the inserts from genomic *B. subtilis* (strain JH642) or *E. coli* (strain MG1655) DNA. Plasmids pPJ1–8 were constructed by ligating a restriction-digested insert into digested pET-21b(+). pPJ9–12 were constructed by ligating restriction-digested insert into the digested pDR67 plasmid. pPJ11–12 plasmids were constructed with forward primers containing the *B. subtilis* ribosome binding site.

For construction of the congeneric *B. subtilis* strains PL3188 (*ftsZ::ftsZ*) and PL3189 (*ftsZ::ftsZ CTVE*), which express wild-type *ftsZ* and *Bs ftsZ CTVE* from the native *ftsZ* promoter, *B. subtilis ftsZ* or *ftsZ CTVE* genes with NdeI/XhoI (New England Biolabs) linkers were amplified from the pPJ1 or pPJ5 plasmids, digested with PstI and XhoI, and ligated into pJL74 (29). The resulting plasmids were transformed into JH642, selecting for single crossover recombination events at the native *ftsZ* locus by growth on spectinomycin-containing media. Mutations were confirmed by plasmid sequencing. Integration was confirmed by chromosomal *ftsZ* locus sequencing.

B. subtilis strains PL3176 and PL3178, which permit depletion of wild-type FtsZ and expression of *E. coli* FtsZ variants, were constructed by first transforming pPJ11 or pPJ12 plasmids into wild-type JH642 cells. This allowed the insertion of a copy of *E. coli ftsZ* or *E. coli ftsZ CTVB* with a *B. subtilis* ribosome-binding site upstream of the start codon at the *amyE* locus under control of the P_{spac} promoter. Chromosomal DNA from the resulting strains was then transformed into competent PL2084 cells (*JH642 thrC::P_{xyI}-ftsZ_{Bs} ftsZ_{Bs}::spc, xylA::tet*), which have their only copy of native FtsZ expressed from a xylose-inducible promoter at the *thrC* locus. This strain permits depletion of wild-type FtsZ and is xylose-dependent for normal growth (30).

Growth Conditions—Growth conditions were as follows. (i) *B. subtilis* congeneric strains PL3188 and PL3189 were grown in LB containing spectinomycin from a single colony overnight and then back-diluted at a 1:100 ratio in fresh LB the next day. Cells were grown to an A_{600} of ~ 0.5 , then back diluted again at a 1:100 ratio in fresh LB and grown until an A_{600} of ~ 0.4 , at which point cells were harvested for analysis via immunofluorescence. (ii) *B. subtilis* strains PL3176 and PL3178 expressing *E. coli* FtsZ variants were first grown from single colony overnight in LB containing spectinomycin and xylose to a final concentration of 0.5%. The next day, cells were diluted 1:100 in fresh LB medium supplemented with 0.5% xylose and grown to an A_{600} of ~ 0.5 , at which point 1 ml of cell culture was harvested by centrifugation. Cells were then washed twice with a fresh 1 ml of LB medium and then diluted 1:100 into a fresh 10 ml of LB medium plus isopropyl 1-thio- β -D-galactopyranoside to a final concentration of 1 mM to induce expression of *E. coli* FtsZs. A_{600} measures were taken every 1 h to monitor cell growth, and at an A_{600} of ~ 0.4 , cells were harvested and prepared for immunofluorescence.

Dilution Plating—Strain PL2452 (*MG1655 leu::Tn10-ftsZ84 (ts)*) transformed with the plasmids pPJ9–12 was used for dilution plating. Cells were grown overnight in LB medium containing ampicillin at 30 °C, and the following morning, cultures were diluted 1:100 into a fresh of 5 ml of low salt (LB with 0.05% NaCl) medium. Cultures were grown at 30 °C until $A_{600} \sim 0.5$, upon which serial dilutions from 10^{-1} to 10^{-8} were made in low salt medium. 10 μ l of each dilution was then plated in series using a multichannel pipette onto either prewarmed LB agar or low salt agar with or without 1 mM isopropyl 1-thio- β -D-galactopyranoside. Liquid cultures were allowed to dry on the plates at room temperature for upwards of 6 h, and then plates were incubated at either the permissive (30 °C) or restrictive (42 °C)

temperature overnight. The plates were then imaged, and relative growth at each temperature was qualitatively assessed.

Immunofluorescence Microscopy—Immunofluorescence was performed as described previously (31). An Olympus BX51 microscope with Chroma filters and a Hamamatsu OrcaERG camera were used for image capture. Images were processed using Openlab version 5.2.2 (Improvision) and Adobe Photoshop CS version 8.0 (Adobe Systems). All cell or ring measurements for collected images were obtained with a minimum population of 200 cells/strain.

B. subtilis FtsZ was detected using affinity-purified polyclonal rabbit anti-FtsZ serum (32) in combination with goat anti-rabbit serum conjugated to Alexa488 (Invitrogen). *E. coli* FtsZ was detected using affinity-purified polyclonal rabbit anti-FtsZ, a gift kindly provided by the William Margolin laboratory, in combination with goat anti-rabbit serum conjugated to Alexa488 (Invitrogen). Cell walls were visualized with wheat germ agglutinin conjugated to tetramethylrhodamine (Invitrogen). Nucleoids were stained with DAPI.

Determination of Cell Length/FtsZ Ring Ratio—The cell length/FtsZ ring (L/R) ratio was calculated as the sum total length of a population of cells divided by the number of FtsZ rings in that population as described previously (33).

Quantitative Immunoblotting—Immunoblotting was done as described previously (30). Briefly, *B. subtilis* cell samples were washed with TE buffer (10 mM Tris (pH 8.0), 1 mM EDTA) and resuspended in lysis buffer (50 mM Tris (pH 8.0), 1 mM EDTA, 100 mM NaCl). Cells were lysed with lysozyme and detergent, and loading was normalized to the A_{600} at sampling. Immunoblot analysis was performed by using affinity-purified polyclonal rabbit anti-FtsZ antibodies (32) and goat anti-rabbit antibodies conjugated to horseradish peroxidase (Jackson ImmunoResearch Laboratories.). Immunoblots were developed by using ECL Western blotting detection reagents (GE Healthcare) and visualized with the luminescent image analyzer ImageQuant LAS 4000 mini (GE Healthcare). Blot density was then quantified using ImageJ, and the linear range for the signal was established from serial dilutions of whole-cell lysates.

Protein Purification—FtsZ variants were cloned into the pET-21b(+) expression vector through *E. coli* strain AG1111. The resulting plasmids were miniprep and freshly transformed into C41(DE3) cells (34) and consequently used for expression of protein. No frozen stocks were used. Briefly, 1 liter of LB medium was inoculated 1:100 with overnight culture from a single colony. Cells were grown at 37 °C until $A_{600} \sim 0.6$, and then cells were induced with isopropyl 1-thio- β -D-galactopyranoside to a final concentration of 1 mM. Cells were grown for an additional 4 h at 37 °C, and then cells were harvested by centrifugation, and cell pellets were stored at -80 °C.

Purification of FtsZs were performed as described previously (31, 35) with the following modifications. After precipitation of FtsZ with ammonium sulfate, FtsZ pellets were resuspended in 50 ml of FtsZ anion exchange buffer (low salt) (50 mM Tris, pH 8.5, 50 mM KCl, 1 mM EGTA, 10% sucrose). The resuspended FtsZ was then filtered through a 0.45- μ m nylon pore membrane. The FtsZ was further purified on a UnoQ6 (Bio-Rad) with a linear gradient of 50–500 mM KCl in 50 mM Tris, pH 8.5, 1 mM EDTA, 10% sucrose. Peak fractions were analyzed by

The C Terminus of FtsZ Mediates Lateral Interactions

TABLE 2

FtsZ GTPase turnover rates

GTPase assays were carried out under conditions identical to those used for light scattering and EM (50 mM MES, pH 6.5, 50 mM KCl, 2.5 mM MgCl₂, 1 mM EGTA, 1 mM GTP, 30 °C). Rates were calculated as GTP consumed/FtsZ subunit/min. Observed FtsZ structures (by EM) are noted in the right column.

FtsZ species	GTP/FtsZ/min	Relative bundling at pH 6.5, 50 mM KCl
Ec FtsZ WT	5.40 ± 0.39	Single filaments
Ec FtsZ ΔC15	4.76 ± 0.29	Single filaments
Bs FtsZ NENDEG	5.85 ± 0.29	Single filaments
Bs FtsZ ΔC17	3.86 ± 0.19	Single filaments
Bs FtsZ CTVE	3.86 ± 0.19	Single filaments
Bs FtsZ NKNRKG	2.32 ± 0.19	Bundled filament sheets
Bs FtsZ WT	2.25 ± 0.40	Filaments sheets and bundled rings
Ec FtsZ CTVB	2.19 ± 0.29	Long filaments, bundles and rings

SDS-PAGE, pooled together, and dialyzed overnight in 1 liter of FtsZ dialysis buffer, pH 7.5 (50 mM HEPES, pH 7.5, 50 mM KCl, 2.5 mM MgCl₂, 1 mM EGTA, 10% sucrose). Protein preparations were concentrated using PEG 12,000, aliquoted, flash frozen on liquid N₂, and stored at -80 °C. Bs FtsZ NENDEG, which has a negatively charged CTV, was precipitated with a single 30% ammonium sulfate cut instead of the 30%/35% cuts used for all other *B. subtilis* FtsZ constructs.

90° Angle Light Scattering Assay—Light scattering experiments were performed essentially as described earlier (31) using a DM-45 spectrofluorimeter (Olis). Readings were taken every 0.25 s at 30 °C, and a base line was established for 1 min prior to the addition of 1 mM GTP. Assembly reactions contained 5 μM FtsZ in assembly buffer (50 mM MES, pH 6.5, 50 mM KCl, 2.5 mM MgCl₂, 1 mM EGTA). Data were collected by SpectralWorks (Olis), exported into Microsoft Excel for processing, and compiled in Kaleidagraph.

Electron Microscopy—Electron microscopy was performed essentially as described (33). 3 μM FtsZ was used because it was found to be the best concentration in which to visualize single FtsZ filaments. FtsZ was assembled with GTP as for light scattering, and samples were visualized using a JEOL 1200EX transmission electron microscope. FtsZ filament lengths were measured using ImageJ, and data were compiled in Microsoft Excel and Kaleidagraph.

GTPase Assay—GTPase activity was measured using the continuous, regenerative coupled GTPase assay of Ingerman and Nunnari (36). Assays were conducted in buffer conditions identical to those used for light scattering. A 150-μl reaction volume included 5 μM FtsZ, 1 mM GTP, 1 mM phosphoenolpyruvate, 250 μM NADH, 80 units/ml lactose dehydrogenase, and 80 units/ml pyruvate kinase. A linear decline of absorbance at 340 nm for NADH was observed at 30 °C for 3 min in a quartz cuvette (1-cm path length) using a SPECTRAMax Plus spectrophotometer (Molecular Devices). The raw data of absorbance per minute were then converted to activity using the extinction coefficient for NADH at 340 nm of 6220 M⁻¹ cm⁻¹. The raw data were then exported to Microsoft Excel for analysis. GTPase data are the average of at least three independent experiments.

Statistical Analyses—Statistical significance was assessed with either unpaired *t* test (GraphPad Quick Calcs; available on the World Wide Web) or one-way analysis of variance. Results were significant if the *p* value was less than 0.05.

RESULTS

FtsZs from both *B. subtilis* and *E. coli* Display Distinct Assembly Properties—Despite a high degree of conservation at the sequence level, particularly in the core domain (54% identical, 76% similar), purified *B. subtilis* and *E. coli* FtsZs behave very differently in standard assays for FtsZ assembly. Transmission electron micrographs of 3 μM FtsZ assembled in our standard FtsZ polymerization buffer (50 mM MES, pH 6.5, 50 mM KCl, 2.5 mM MgCl₂, 1 mM EGTA, 1 mM GTP) indicate that *B. subtilis* FtsZ (Bs FtsZ) has a strong propensity to form stable lateral interactions, whereas *E. coli* FtsZ (Ec FtsZ) does not (Fig. 2). Bs FtsZ formed both large bundles of filament rings (Fig. 2A) and sheets of single-stranded filaments (protofilaments) (Fig. 2B), whereas Ec FtsZ was found primarily as unbundled single-stranded filaments (Fig. 2C). Ec FtsZ filaments were also longer than Bs FtsZ filaments, averaging 218.88 ± 56.54 nm in length versus 129.32 ± 36.33 nm for their *B. subtilis* counterparts (Fig. 2F).

Consistent with the presence of increased lateral interactions and larger structures, Bs FtsZ produces a 23-fold higher signal than Ec FtsZ when assembly is assayed by 90° angle light scattering (Fig. 2G). 90° angle light scattering is a standard method to measure FtsZ assembly in real time (5). The nature of the assay is such that highly bundled polymers will produce a larger signal than the same number of unbundled single-stranded polymers due to increased polymer mass (5). In light of our EM data, we therefore interpret the large difference in light scattering signal between the Bs FtsZ and Ec FtsZ to be a reflection of the increased lateral interactions between Bs FtsZ filaments. In agreement with previous studies, both Bs FtsZ and Ec FtsZ assemble in a GTP-dependent manner, reaching steady state approximately 1 min after the addition of GTP (5, 37) (Fig. 2, G and H).

The differences in bundling appear to be electrostatically driven because increasing the KCl concentration in the buffer lowers the Bs FtsZ light scattering signal ~40-fold, whereas that of Ec FtsZ is largely unaffected (supplemental Fig. S1). In the same buffer used to measure FtsZ assembly, Bs FtsZ hydrolyzed GTP at a rate of 2.25 ± 0.40 GTP/FtsZ/min, whereas Ec FtsZ hydrolysis was 5.40 ± 0.39 GTP/FtsZ/min. The GTPase rate of Bs FtsZ is significantly lower than that of Ec FtsZ, presumably due to reduced turnover of subunits in bundled protofilaments of Bs FtsZ (Table 2).

Note that the same polymerization buffer is used throughout this study. Ec FtsZ has been reported to form structures several

protofilaments thick in the presence of higher levels of magnesium, 10 mM MgCl₂ (38, 39). Mg²⁺, along with Ca²⁺ and the molecular crowding agent DEAE-dextran, has been shown to stimulate lateral interactions and the formation of higher order structures (40). However, the 2.5 mM concentration of Mg²⁺ in our standard polymerization buffer is more physiologically relevant (41). All EM was conducted with FtsZ at a concentration of 3 μM to allow us to visualize single-stranded filaments more easily, and light scattering and GTPase assays were performed at a concentration of 5 μM.

Deletion of Conserved C-terminal Tail Eliminates *B. subtilis* FtsZ Lateral Interactions—In light of these findings, we next sought to determine which regions of FtsZ might account for the differences in the ability of Bs FtsZ and Ec FtsZ to bundle. Because the N-terminal core domain is relatively well conserved between *E. coli* and *B. subtilis*, we speculated that the C-terminal region, particularly the CTT and CTV, might account for the difference in assembly properties. Although the role of the CTT in interactions with FtsZ modulatory proteins has been studied in some depth (18, 20, 22, 23), a function for the C terminus in FtsZ polymer assembly in the absence of modulatory proteins has not been established.

To determine the role of the CTT and CTV in FtsZ assembly, we engineered a *B. subtilis* FtsZ protein that is missing the last 17 residues starting at Asp-366, a region that includes both the CTT and the CTV (Bs FtsZ ΔC17). Because most of the longitudinal contacts between adjacent FtsZ subunits have been mapped to the N-terminal core (15, 17), we hypothesized that the Bs FtsZ ΔC17 mutant would still be able to assemble into protofilaments and maintain GTPase activity needed for oligomerization. Bs FtsZ ΔC17 and all other FtsZ constructs used in this work are depicted in Fig. 1C.

Our data suggest that the C terminus of *B. subtilis* FtsZ plays an important role in assembly (Fig. 2, D and G). EM images of Bs FtsZ ΔC17 assembled in the presence of GTP indicate that it is almost exclusively in single-stranded protofilaments. Consistent with a lack of bundling, Bs FtsZ ΔC17 reached maximal assembly at only 1.8% of the peak value of Bs FtsZ WT (Fig. 2, G and H). Similarly, the GTP turnover rate of Bs FtsZ ΔC17 was 71% higher than that of wild-type Bs FtsZ, although not as high as that observed for Ec FtsZ, which also displays unbundled single filaments (Table 2). Bs FtsZ ΔC17 filaments averaged 107.26 ± 37.84 nm in length, significantly shorter than Bs FtsZ WT (Fig. 2F).

In contrast to *B. subtilis* FtsZ, deleting the last 15 residues of *E. coli* FtsZ (residues 369–383), the region constituting its CTT and CTV, had only a small impact on assembly. Like wild-type Ec FtsZ, Ec FtsZ ΔC15 readily assembled into single protofilaments upon the addition of GTP, and no bundling was observed (Fig. 2E). The Ec FtsZ ΔC15 filaments, however, were somewhat shorter than wild-type Ec FtsZ (182.35 ± 47.67 nm in length versus 218.88 ± 56.54 nm) (Fig. 2F). The average peak light scattering value for Ec FtsZ ΔC15 was 83% of wild-type Ec FtsZ ($p < 0.05$), consistent with the reduction in average filament length (Fig. 2H). GTP hydrolysis rates of Ec FtsZ ΔC15 were near that of wild-type Ec FtsZ, with average values of 4.76 ± 0.29 GTP/FtsZ/min and 5.40 ± 0.39 GTP/FtsZ/min, respectively ($p > 0.05$) (Table 2).

***B. subtilis* FtsZ CTV Is Sufficient to Induce Lateral Interactions between FtsZ Protofilaments**—Based on our finding that the C terminus of Bs FtsZ was required for lateral interactions *in vitro*, we next investigated the role of the CTV in this process. In contrast to the highly conserved CTT, the CTV is highly variable both in length and content between FtsZs from different species. To test the role of the CTV in modulating lateral interactions, we swapped the last 6 residues of Bs FtsZ with the last 4 residues of *E. coli* FtsZ. The fusion boundaries for the chimeric proteins were at the very end of the CTT, Arg-376 in Bs FtsZ and Arg-379 in Ec FtsZ (Fig. 1C). We designated the resulting chimeras Bs FtsZ CTVE and Ec FtsZ CTVB.

Data from the chimeric proteins supports a central role for the CTV in modulating lateral interactions. Under standard polymerization conditions, Bs FtsZ CTVE was able to form single-stranded polymers; however, no FtsZ filament bundles were observed (Fig. 3A). Consistent with the EM data, Bs FtsZ CTVE exhibited a peak light scattering value on par with that of Bs FtsZ ΔC17 and only 1.65% of the peak light scattering value of wild-type Bs FtsZ (Fig. 3E). Similarly, the GTPase turnover rate of Bs FtsZ CTVE was essentially equivalent to Bs FtsZ ΔC17 (3.86 ± 0.19 GTP/FtsZ/min), significantly higher than wild-type Bs FtsZ (2.25 ± 0.40 GTP/FtsZ/min) ($p < 0.005$). Average Bs FtsZ CTVE filament lengths measured 95.92 ± 22.16 nm, shorter than the 129.32 ± 36.33 nm observed for Bs FtsZ (Fig. 3D).

Data from Ec FtsZ CTVB indicates that the CTV from *B. subtilis* is sufficient to promote lateral interactions between single-stranded FtsZ polymers. In contrast to both wild-type *E. coli* FtsZ and Bs FtsZ CTVE, the Ec FtsZ CTVB chimera readily formed lateral interactions *in vitro* (Fig. 3B). In the presence of GTP, purified Ec FtsZ CTVB formed thick filament sheets as well as rings and toroidal structures (Fig. 3C). Such structures have previously been observed for Ec FtsZ only in the presence of higher concentrations of divalent cations or molecular crowding agents (7). The diameter of the Ec FtsZ CTVB rings was on average 370.64 ± 46.24 nm with a width of 58.27 ± 20.37 nm, somewhat larger than those observed for a similar structure composed of wild-type Bs FtsZ (183.41 ± 34.27-nm diameter; 30.66 ± 10.85-nm width) (supplemental Fig. S2D).

Consistent with increased lateral interactions and the presence of very large macromolecular weight complexes, Ec FtsZ CTVB had a peak light scattering value ~30-fold higher than wild-type Ec FtsZ and ~30% greater than Bs FtsZ (Fig. 4E). The GTPase turnover rate of the Ec FtsZ CTVB was significantly lower than wild-type Ec FtsZ at only 2.19 ± 0.29 GTP/FtsZ/min, also consistent with an increase in lateral interactions. Individual Ec FtsZ CTVB protofilaments were typically longer than wild-type Ec FtsZ (277.58 ± 49.40 nm versus 218.88 ± 56.54 nm) (Fig. 3D), and the range of lengths was significantly broader (supplemental Fig. S2).

CTV Charge Plays Critical Role in Lateral Interaction Potential—At pH 6.5, the Bs FtsZ CTV (NRNKRK) is highly positive, whereas the Ec FtsZ CTV (KQAD) has a net neutral charge. We therefore speculated that the positive charge of the Bs FtsZ CTV conferred the ability in Bs FtsZ to form lateral filament interactions. To test this possibility, we examined the assembly properties of two Bs FtsZ mutants,

The C Terminus of FtsZ Mediates Lateral Interactions

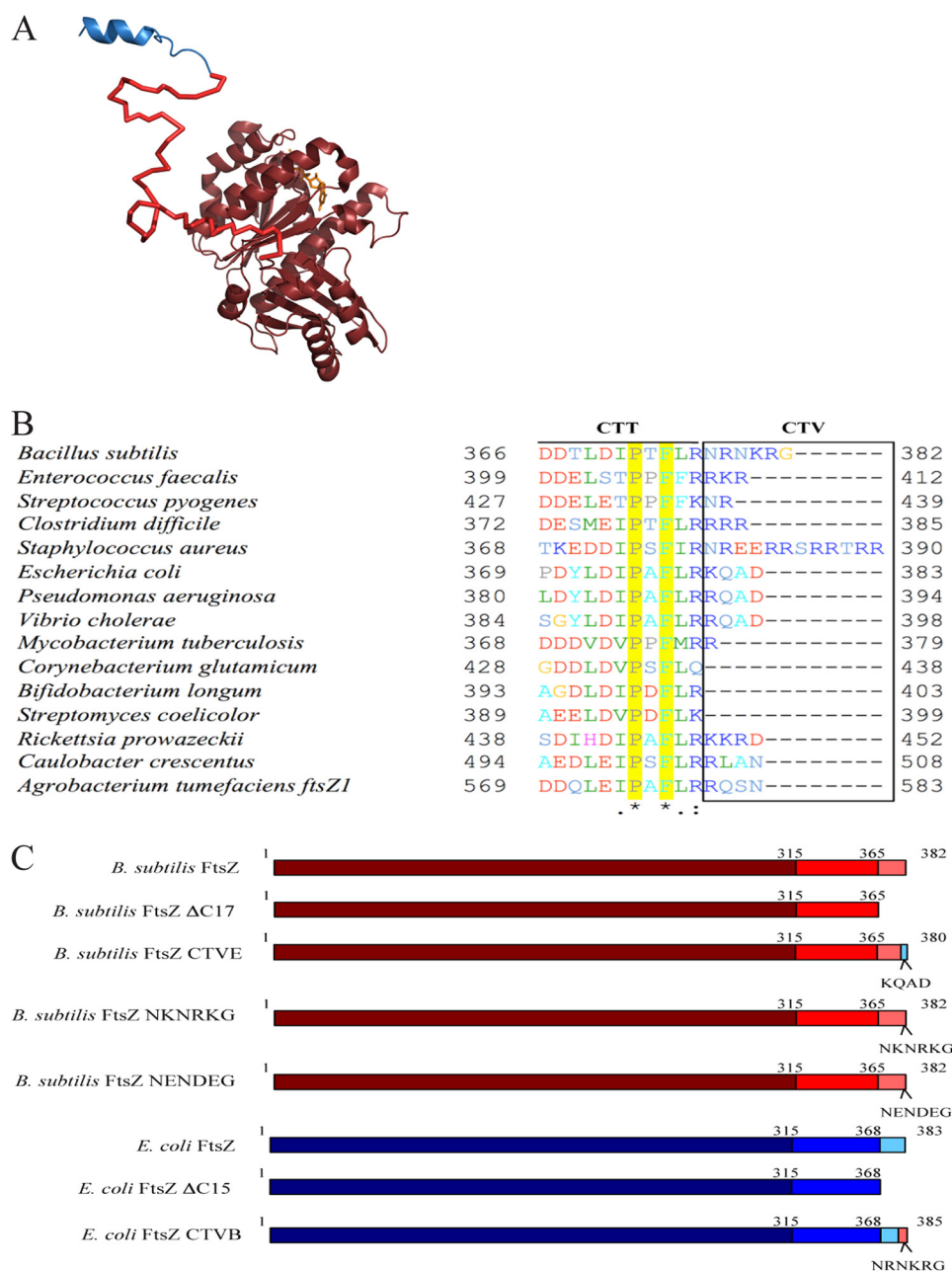


FIGURE 1. FtsZ domain structure, C-terminal alignments, and protein constructs. *A*, structure of *B. subtilis* FtsZ showing the N-terminal core in maroon bound to GDP (from Protein Data Bank entry 2RHO (59)). The flexible C-terminal linker (red) is depicted here as an unstructured peptide. The conserved CTT, in blue, is depicted as a short α -helix based on the structure of the *E. coli* CTT in complex with ZipA (19). *B*, alignment of the FtsZ C termini from 15 different organisms. Conserved in all organisms, a proline (*B. subtilis* position 372) and phenylalanine (*B. subtilis* position 374) are highlighted in yellow. The CTV is boxed. *C*, schematic of the different FtsZ constructs used in this study, drawn to scale.

one in which the positive charge of the CTV was conserved but replaced with different amino acids (Bs FtsZ NKNRKG) and another in which the charges were completely reversed (Bs FtsZ NENEDEG).

Our data suggest that CTV charge is the primary determinant of Bs FtsZ lateral interaction potential. Although the positively charged Bs FtsZ NKNRKG mutant readily formed filament bundles and sheets *in vitro*, the negatively charged Bs FtsZ NENEDEG did not (Fig. 4, *A* and *B*). Similarly, in light-scattering reactions, Bs FtsZ NKNRKG assembled robustly, albeit 2-fold less than wild-type Bs FtsZ. However, the light scattering signal of negatively charged Bs FtsZ NENEDEG was \sim 16-fold less

than that of wild-type Bs FtsZ (Fig. 4*D*), a level comparable with Ec FtsZ and Bs FtsZ Δ C17.

Although the positively charged Bs FtsZ NKNRKG readily formed bundles *in vitro* (Fig. 4*A*), we did not observe any of the bundled ring structures characteristic of wild-type Bs FtsZ, suggesting a possible role for specific CTV residues in mediating lateral interactions. This finding is consistent with the somewhat reduced signal of this mutant in the light scattering reaction (Fig. 4*D*). Filaments averaged a length of 133.67 ± 37.42 nm (Fig. 4*C*).

GTPase data reflect the relative lateral interaction potential of the two FtsZ mutants. Negatively charged Bs FtsZ NENE-

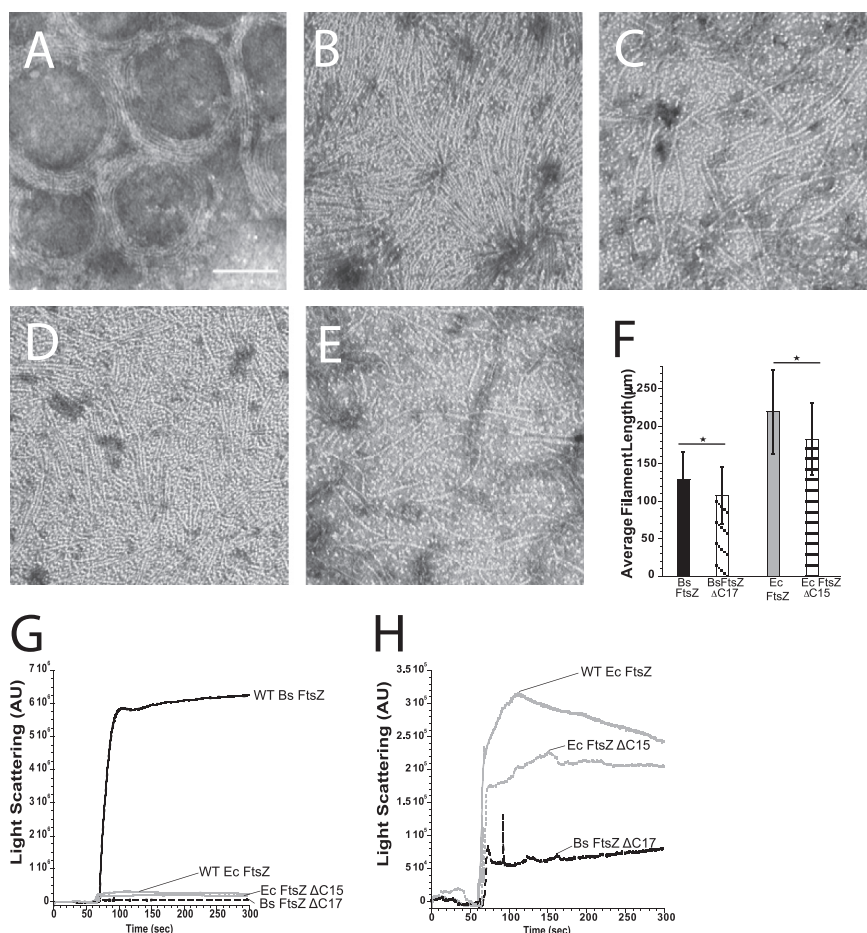


FIGURE 2. The *B. subtilis* FtsZ C terminus is required for lateral interactions *in vitro*. *A–E*, electron micrographs of 3 μM FtsZ assembled in the presence of GTP. *Bar*, 100 nm. *A*, bundled rings of Bs FtsZ. *B*, ordered sheets of Bs FtsZ filaments on the same grid as *A*. *C*, in the presence of GTP, Ec FtsZ assembles into more or less randomly positioned single-stranded filaments. *D*, in contrast to full-length Bs FtsZ, Bs FtsZ ΔC17 assembles into predominantly single-stranded filaments. *E*, Ec FtsZ ΔC15 assembles into predominantly single filaments that are indistinguishable from full-length Ec FtsZ. *F*, average filament lengths. Bs FtsZ ΔC17 (black diagonal stripes) and Ec FtsZ ΔC15 filaments (black horizontal bars) (107.26 \pm 37.84 and 182.35 \pm 47.67 nm, respectively) are significantly shorter than full-length Bs FtsZ (solid black) and Ec FtsZ (solid gray) (129.32 \pm 36.33 and 218.88 \pm 56.54 nm, respectively). More than 100 filaments were measured for each FtsZ. *Error bars*, S.D. *G*, representative traces of 5 μM FtsZ assembled in the presence of GTP and measured by 90° angle light scattering. Bs FtsZ ΔC17 and Ec FtsZ show \sim 90- and \sim 23-fold decreases in light scattering signal relative to Bs FtsZ, respectively. The Ec FtsZ ΔC15 signal is reduced by 17 percent compared with the wild-type Ec FtsZ. *H*, same plot as in *G* but scaled to highlight GTP-dependent increase in light scattering of Ec FtsZ, Bs FtsZ ΔC17 , and Ec FtsZ ΔC15 . Note that buffer conditions for all *in vitro* work were as follows: 50 mM MES, pH 6.5, 50 mM KCl, 2.5 mM MgCl₂, 1 mM EGTA, 1 mM GTP. FtsZ was used at a concentration of 3 μM for all electron microscopy to facilitate visualization of single-stranded polymers. For 90° angle light scattering and GTPase assays, FtsZ concentration is always 5 μM . *AU*, arbitrary units. *, $p < 0.001$.

DEG had elevated GTPase activity with a rate of 5.85 \pm 0.29 GTP/FtsZ/min, comparable with that of Ec FtsZ. In contrast, positively charged Bs FtsZ NKNRKG exhibited a rate of 2.32 \pm 0.19 GTP/FtsZ/min, in the range of wild-type Bs FtsZ. Despite its inability to form lateral interactions, the average filament length of negatively charged Bs FtsZ NENDEG was 176.00 \pm 51.64 nm, significantly longer than the average for wild-type Bs FtsZ (129.32 \pm 36.33 nm).

Defects in Lateral Interaction Potential Impair Cell Division in *B. subtilis*—To determine if the lateral interactions we observed for *B. subtilis* FtsZ *in vitro* (Fig. 2*A*) were relevant *in vivo*, we engineered an otherwise wild-type *B. subtilis* strain expressing Bs FtsZ CTVE from the native FtsZ promoter (see “Experimental Procedures”). As a control, we engineered a congenic strain expressing wild-type *Bs ftsZ*. Cells were grown to mid-exponential phase ($A_{600} \sim 0.4$), fixed, stained for cell wall and FtsZ, and visualized by fluorescence microscopy. Quanti-

tative Western blot analysis demonstrated the mutant FtsZ CTVE construct is stable *in vivo* (supplemental Fig. S4)

Analysis of *Bs ftsZ* CTVE mutants suggests that the lateral interactions we observed *in vitro* are critical for FtsZ ring integrity *in vivo* and support a role for the CTV in stabilizing FtsZ polymers within the cytokinetic ring. Although *B. subtilis* cells expressing *Bs ftsZ* CTVE grew normally and exhibited exclusively medial FtsZ rings (Fig. 5*A*), they were on average \sim 85% longer than congenic wild-type cells (Fig. 5*D*). \sim 31% (90 of 290) of *Bs ftsZ* CTVE mutants were filamentous (>5 cell lengths), suggesting that cells expressing the chimera failed to divide at a relatively high frequency.

Comparisons of cell length (*L*) with the number of FtsZ rings (*R*) indicated that the *L/R* ratio of the *Bs ftsZ* CTVE mutants was nearly 75% greater than wild-type cells. Whereas the congenic wild-type strain had an *L/R* ratio of 7.42 \pm 0.71 $\mu\text{m}/\text{ring}$, similar to that of wild-type JH642 cells (33), *Bs ftsZ* CTVE mutants

The C Terminus of FtsZ Mediates Lateral Interactions

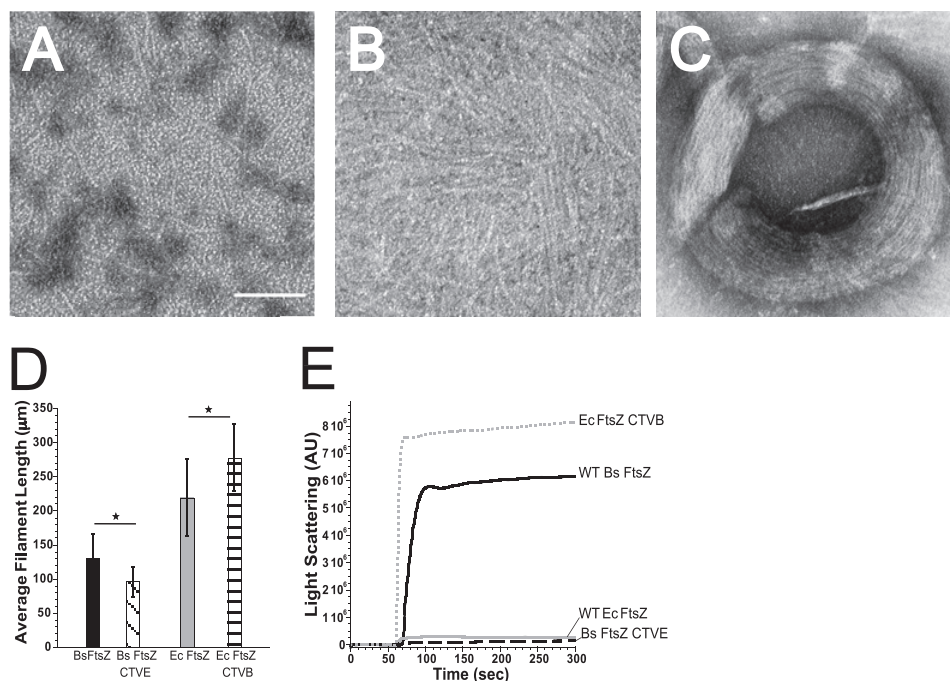


FIGURE 3. The *B. subtilis* CTV is sufficient to promote lateral interactions *in vitro*. A–C, electron micrographs of Bs FtsZ CTVE and Ec FtsZ CTVB assembled in the presence of GTP. Bar, 100 nm. A, Bs FtsZ CTVE forms predominantly short single-stranded filaments with little evidence of lateral interactions. B, Ec FtsZ CTVB forms large sheets consistent with extensive lateral interactions. C, Ec FtsZ CTVB filament bundle. D, average filament lengths of Bs FtsZ CTVE (diagonal black stripes) and Ec FtsZ CTVB (horizontal black stripes) (95.92 ± 22.16 and 277.58 ± 49.40 nm, respectively) are significantly shorter than wild-type Bs FtsZ (solid black) and Ec FtsZ (solid gray) (129.32 ± 36.33 and 218.88 ± 56.54 nm, respectively). More than 100 filaments were measured for each FtsZ. Error bars, S.D. E, representative traces of $5 \mu\text{M}$ FtsZ assembled in the presence of GTP and measured by 90° angle light scattering. Note the 60-fold decrease in light scattering signal of Bs FtsZ CTVE relative to wild-type Bs FtsZ and the 30-fold increase in signal of Ec FtsZ CTVB relative to wild-type Ec FtsZ. AU, arbitrary units. *, $p < 0.001$.

had a L/R ratio of $12.97 \pm 0.40 \mu\text{m}/\text{ring}$, consistent with a reduction in the frequency of FtsZ ring formation (Fig. 5C).

Not surprisingly, none of the CTV chimeras were able to support division outside of their native species, in support of previous work (17). Neither wild-type Ec FtsZ nor Ec FtsZ CTVB supported division in *B. subtilis* cells depleted for wild-type Bs FtsZ (Fig. 5E). Both Ec FtsZ and Ec FtsZ CTVB were dispersed throughout the cytoplasm, suggesting that they lacked a targeting determinant required for medial localization and/or failed to interact with critical cell division proteins. Bs FtsZ and Bs FtsZ CTVE expressed from a plasmid vector were similarly unable to rescue cell division in the heat-sensitive *E. coli ftsZ84* mutant at the restrictive temperature (supplemental Fig. S3).

DISCUSSION

Taken together, our data strongly support a role for the FtsZ C terminus, particularly the poorly conserved residues at the very end of the protein (the CTV), in modulating lateral interactions between protofilaments in the absence of modulatory proteins. Specifically, we find that the last 6 residues of *B. subtilis* FtsZ are both necessary and sufficient to promote the high degree of lateral interactions characteristic of wild-type *B. subtilis* FtsZ. Swapping the 6-residue CTV of *B. subtilis* FtsZ with the 4-residue *E. coli* FtsZ CTV reverses the bundling potential of both proteins, reducing the light scattering signal 60-fold for Bs FtsZ and increasing it 30-fold for Ec FtsZ (Fig. 3). Importantly, *B. subtilis* FtsZ CTVE has a significant cell division defect *in vivo*, strongly supporting the physiological relevance of our biochemical data.

Although the CTT has been implicated in interactions between FtsZ and modulatory proteins (15, 16, 42, 43), the role of the FtsZ C terminus in FtsZ assembly has not been subject to direct analysis until this work. Below we discuss the implication of these findings with regard to our understanding of the mechanisms driving FtsZ lateral interactions both alone and in the presence of modulatory proteins.

Electrostatic Forces as Primary Determinant of Lateral Interaction Potential—Our findings support a model in which CTV charge is the primary determinant of its effect on bundling. Both wild-type Bs FtsZ and one in which positively charged residues in the CTV have been replaced by residues with similar charge exhibit a high degree of lateral interaction potential and low GTPase activity (Figs. 2 and 4). Conversely, Bs FtsZ mutants in which the positively charged wild-type CTV was replaced with either the neutral CTV from *E. coli* FtsZ or a negatively charged CTV sequence, NENDEG, were more or less equivalent to wild-type *E. coli* FtsZ with regard to bundle formation, light scattering, and GTPase activity (Figs. 3 and 4). In other words, whereas a positively charged CTV appears to be an indicator of a high degree of lateral interaction potential, a negative or neutral CTV is suggestive of a low level of lateral interaction potential.

In light of these findings, we propose a model in which the FtsZ filament is in essence a linear polyelectrolyte separate from the flexible linker, CTT, and CTV. The cores of both Bs FtsZ and Ec FtsZ carry a net negative charge at physiological pH. Whereas a negatively charged or neutral CTV would have little impact on lateral interactions between negatively

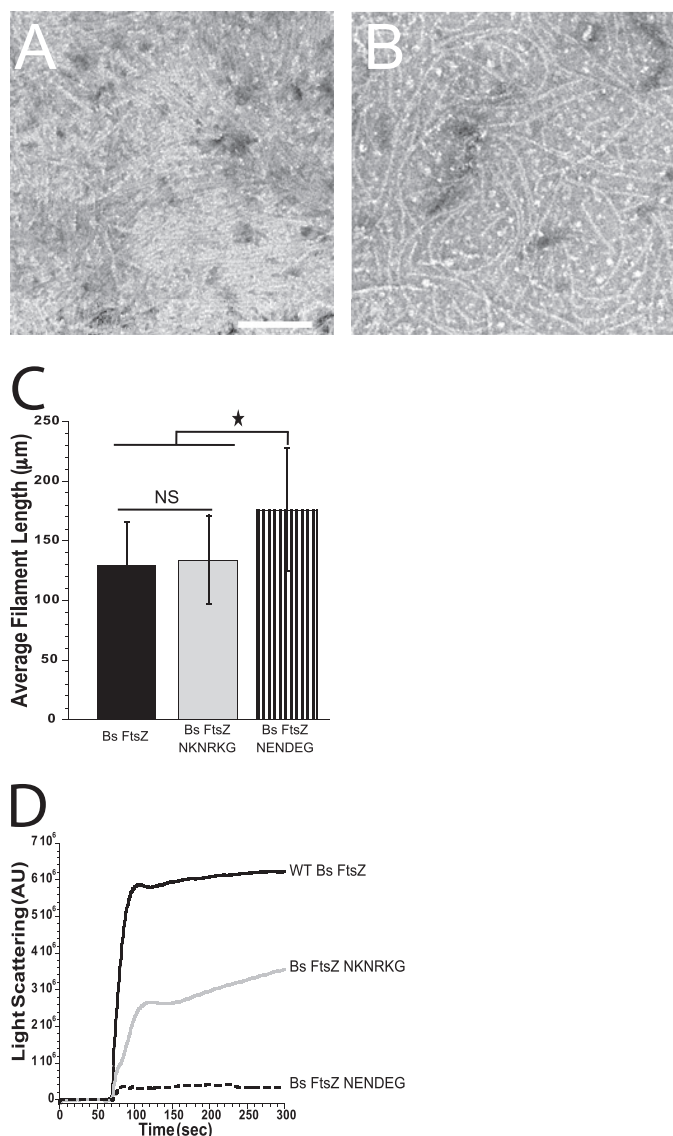


FIGURE 4. Bs FtsZ CTV charge appears to be the primary determinant of lateral interaction potential. *In vitro* assembly of *B. subtilis* FtsZ NKNRKG (positively charged CTV) and *B. subtilis* FtsZ NENDEG (negatively charged CTV). *A* and *B*, electron micrographs of 3 μm Bs FtsZ NKNRKG and Bs FtsZ NENDEG. Bar, 100 nm. *A*, Bs FtsZ NKNRKG assembled into filament bundles running across the width of the field. Note ordered sheet visible in bottom right corner. *B*, single filaments of Bs FtsZ NENDEG. *C*, the average filament lengths of Bs FtsZ NKNRKG (solid gray) are similar to wild-type Bs FtsZ (solid black) (133.67 ± 37.42 versus 129.32 ± 36.33 nm), whereas Bs FtsZ NENDEG (black stripes) filaments measuring 176.00 ± 51.64 nm are significantly longer (one-way analysis of variance with $\alpha = 0.001$). More than 100 filaments were measured per FtsZ. Error bars, S.D. *D*, representative traces of 5 μm FtsZ assembled in the presence of GTP and measured by 90° angle light scattering. AU, arbitrary units. *, $p < 0.05$; NS, not significant.

charged strands, a positively charged CTV would function as a polycation, shielding adjacent, negatively charged filaments from one another and thus facilitating lateral interactions. Data indicating that increasing the salt concentration of the polymerization buffer also inhibits lateral interactions between polymers of Bs FtsZ further support this model (supplemental Fig. S1).

High concentrations of other charged ions, for instance Ca^{2+} and Mg^{2+} , also favor protofilament bundling in Ec FtsZ even in the absence of the CTT and CTV (44). We have observed a

similar phenomenon for Bs FtsZ,³ suggesting that the cations play a charge-shielding role similar to that played by the CTV to promote bundling in its absence.

Modulatory proteins that promote lateral interactions between FtsZ protofilaments, such as ZapA and *B. subtilis* SepF may function by mimicking the positively charged CTV. Consistent with this idea, data from the crystal structure of ZapA suggest the ZapA tetramer has an exposed patch of positive residues in its more conserved globular domain (45). Depending on its orientation relative to the FtsZ polymer, it is possible that the charged patch of ZapA might promote bundling by shielding negatively charged FtsZ cores on adjacent polymers, in a manner similar to the model we propose for the Bs FtsZ CTV. More work is needed, however, to detail electrostatic potential of the SepF protein.

Although charge appears to be the primary determinant of lateral interaction potential, other forces cannot be ruled out as contributors to FtsZ bundling. A conservative change in Bs FtsZ CTV (NRNKRK to NKNRKG) that altered amino acid composition but retained the positively charged nature of the Bs CTV reduced the light scattering signal 2-fold, although sheets and smaller bundles were still readily visible by EM (Fig. 4, *A* and *D*). This finding suggests that other factors, such as salt bridges between specific residues or van der Waals interactions, may also play a role in FtsZ filament bundling.

In support of the idea that specific interactions between residues in the CTV and the core contribute to bundle formation, a handful of residues on the surface of the FtsZ core have been implicated in modulating lateral interactions (15, 16, 42, 43) (supplemental Table S1). Specifically which core residues might interact with the CTV is not clear. Based on our observation that the Bs FtsZ CTV is sufficient to enhance bundling of Ec FtsZ 30-fold, we would predict that the Bs FtsZ CTV interacts with conserved residues on the core of Ec FtsZ (Fig. 3). To date, however, either core residues implicated in lateral interactions are not well conserved between *B. subtilis* and *E. coli* FtsZs (15), or mutants in these residues are significantly deficient in GTPase activity (43), suggesting that longitudinal interactions between subunits are perturbed in contrast to our Bs FtsZ ΔC17 and Bs FtsZ CTVE mutants (supplemental Table S1).

Filament Length Appears to Be Independent of Lateral Interaction Potential—Somewhat surprisingly, we did not observe a strong correlation between filament length and lateral interaction potential. Although the relationship between filament length and bundling is not well understood, it has been addressed through modeling (46). At steady state, lateral interactions are predicted to be more favorable as filament length increases. This was the observed case for our Ec FtsZ CTVB mutant, which bundled with high efficiency and had significantly longer filaments than wild-type Ec FtsZ *in vitro* (Fig. 3D). However, this notion does not apply when comparing Bs FtsZ with Ec FtsZ. Generally, the better bundling Bs FtsZ had average single filament lengths less than the single-stranded Ec FtsZ as did the poorly bundling Bs FtsZ ΔC17 and Bs FtsZ CTVE

³ P. J. Buske and P. A. Levin, unpublished observation.

The C Terminus of FtsZ Mediates Lateral Interactions

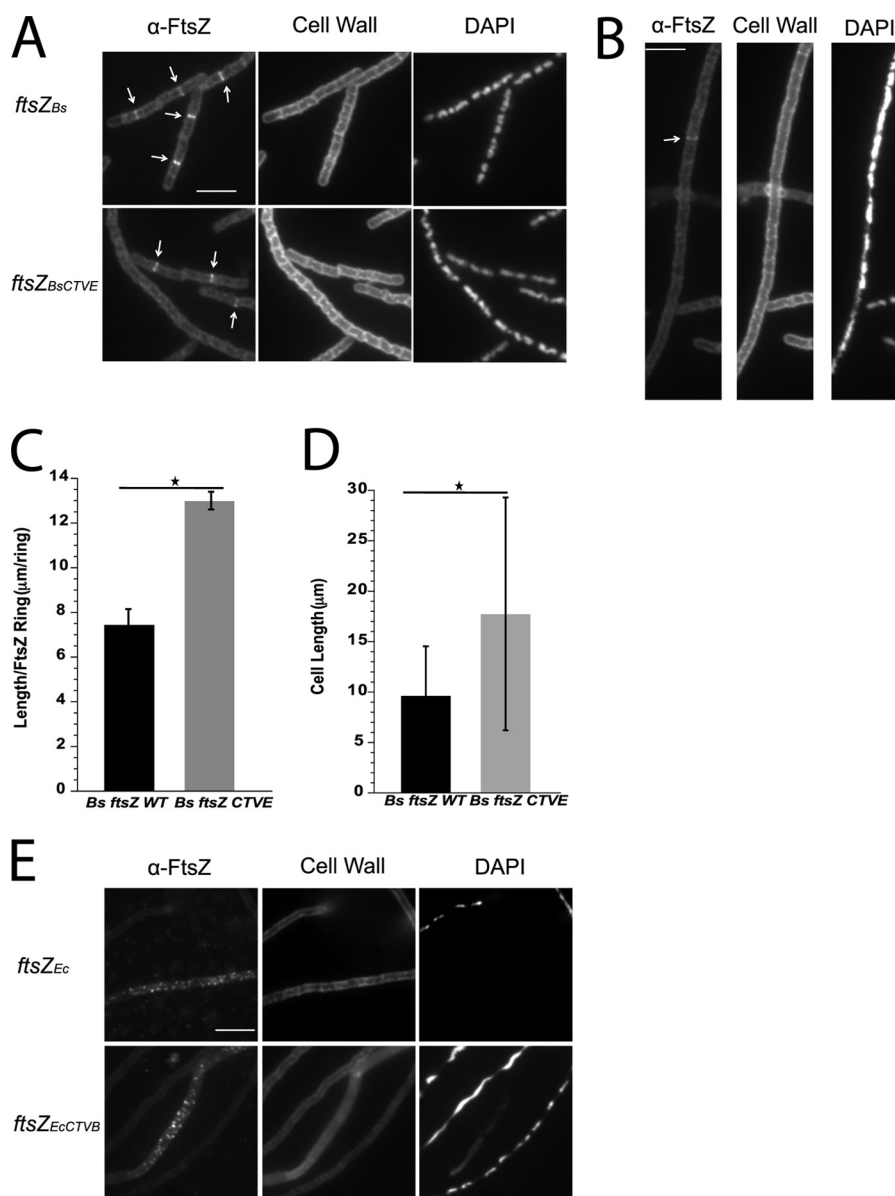


FIGURE 5. The FtsZ CTV plays a critical role in maintenance of FtsZ ring integrity *in vivo*. *A*, immunofluorescence microscopy of cells expressing *Bs ftsZ* (top) and *Bs ftsZ CTVE* (bottom). *Bs ftsZ CTVE* assembles into rings at midcell (arrows) and supports division. *B*, ~31 percent (90 of 290) of *Bs ftsZ CTVE* mutants were filamentous (>5 cell lengths) consistent with a reduction in FtsZ ring integrity. The arrow highlights that the Z-ring within filament of cells still occurs. *C*, the length/FtsZ ring (L/R) ratio of *Bs ftsZ CTVE* cells (gray bar) is ~75 percent higher than that of *Bs ftsZ WT* cells (black bar). Error bars, S.D. The *Bs ftsZ CTVE* error bar is large, reflecting the high heterogeneity of cell lengths in the population. *D*, *Bs ftsZ CTVE* cells (gray bar) are ~85 percent longer than congenic *Bs ftsZ WT* cells (black bar). Error bars, S.D. *E*, neither *Ec ftsZ* nor *Ec ftsZ CTVB* support division in *B. subtilis* cells depleted for wild-type FtsZ. Note the punctate localization of *Ec ftsZs*, indicating failure to localize to midcell. Bar, 5 μm . *, $p < 0.001$.

variants (Fig. 2*F*). The possibility exists that there could very well be intrinsic length limits to FtsZ filaments from different species. This idea is supported by looking at the lengths of our *Bs ftsZ* Δ C17 and *Ec ftsZ* Δ C15 mutants (Fig. 2*F*). *Bs ftsZ* Δ C17 had significantly shorter single filament lengths than *Ec ftsZ* Δ C15, indicating that length is not dependent on the ability of the FtsZ to bundle.

Regardless of species, deleting the C termini (CTT and CTV) of either *B. subtilis* or *E. coli* FtsZ significantly reduced the average length of single-stranded polymers (Fig. 2*F*), suggesting a possible role for this region in modulating interactions between subunits within individual protofilaments. For example, the C terminus may increase nucleation rates without altering elon-

gation rates, a situation that would lead to the formation of a higher number of shorter filaments due to an overall reduction in the pool of FtsZ subunits available for assembly. Regardless of mechanism, our findings highlight the need for closer examination of the assembly dynamics of both wild-type FtsZ and C-terminal deletion mutants, to illuminate the factors that contribute to FtsZ filament length.

Changes in Lateral Interaction Potential in Vitro Impact FtsZ Ring Stability in Vivo—Our data support a model for cell division in which lateral interactions between protofilaments are important *in vivo*. The high ionic strength and pH of the cytoplasm differ from our *in vitro* conditions and are likely to weaken the ability of the positively charged CTV to promote

lateral interactions to some degree. However, *B. subtilis* cells expressing the poorly bundled Bs FtsZ CTVE chimera as the sole copy of FtsZ exhibited a mild cell division defect, suggesting that the wild-type CTV plays a role in modulating lateral interactions *in vivo*. Bs FtsZ CTVE mutant cells were on average ~85% longer than congenic cells expressing wild-type FtsZ, exhibited a high frequency of filamentation, and had an elevated cell length/FtsZ ring ratio (Fig. 5, A and B), consistent with a reduction in the integrity of the FtsZ ring. Over 30% of Bs *ftsZ* CTVE mutants were filaments, suggesting that at least a subset of these cells is at the precipice between being able to divide and failure of the division machinery.

Although we do not favor the possibility, the Bs *ftsZ* CTVE cell division phenotype may be due to a loss of interaction between FtsZ and a modulatory protein that interacts with the CTV. A potential candidate for such a modulatory protein is FtsA, which helps to anchor FtsZ to the membrane through interactions with CTT (3, 18, 20, 47). In support of this idea, an *ftsA* deletion in *B. subtilis* also leads to a mild to moderate cell division defect (48). However, the length of Bs *ftsZ* CTVE mutant cells is significantly more variable than that of *ftsA* deletion mutants. Similarly, although we observed irregular FtsZ localization in the Bs FtsZ CTVE mutant (Fig. 5), consistent with a disruption in Z-ring integrity, Z-rings are regularly positioned in the *ftsA* deletion, and although irregular in shape, Z-rings are still assembled (48). Moreover, there are no data suggesting that FtsA interacts directly with residues in the CTV of either *E. coli* FtsZ or *B. subtilis* FtsZ. Finally, although it is possible that the CTV is needed for an interaction with a modulatory protein other than FtsA, it is unclear what such a protein would be because the Bs *ftsZ* CTVE phenotype is unlike those of other cell division mutants, including *zapA* and *sepF* (6, 49).

Thus far, the native CTT is the primary location for interactions between FtsZ and its regulatory proteins, and it is unchanged in the Bs *ftsZ* CTVE mutant. We therefore favor the more straightforward explanation that our *in vivo* and *in vitro* phenotypes are related.

What is perhaps more surprising is that Bs FtsZ CTVE is able to support division at all, given its relatively poor ability to bundle *in vitro*. In this way, the Bs *ftsZ* CTVE mutant is reminiscent of two other FtsZ mutants, *ts1* from *B. subtilis* and *ftsZ84* from *E. coli*. Purified *E. coli* FtsZ84 is unable to assemble to a significant degree *in vitro* and is moderately defective in GTP binding and hydrolysis (although it is able to bind and hydrolyze ATP as well) (17, 50). However, *in vivo* the *ftsZ84* mutation is able to support division at the permissive temperature of 30 °C and/or in the presence of NaCl (51, 52). Similarly, although the conditional *B. subtilis* mutant FtsZ(Ts1) is unable to form lateral interaction *in vitro*, it is capable of supporting division *in vivo* at permissive temperatures (42). We speculate that in all three cases, the Bs FtsZ CTVE, FtsZTs1, and FtsZ84 mutant proteins retain their ability to interact with modulatory proteins, which in turn promote stabilizing lateral interactions, thereby ameliorating any assembly defect *in vivo*. Consistent with this hypothesis, overexpression of the stabilizing protein ZipA represses the thermosensitivity of the *ftsZ84* mutant at 42 °C (53).

Our finding that neither the wild-type Ec FtsZ nor the Ec FtsZ CTVB chimera was able to support division in *B. subtilis* (Fig. 5E) is consistent with previous work indicating that *B. subtilis* FtsZ is unable to support division in wild-type *E. coli* (17, 54). Moreover, the wild-type *E. coli* FtsZ and *E. coli* FtsZ CTVB that we observed in *B. subtilis* cells depleted for native FtsZ (Fig. 5E) are strikingly similar to the foci generated by expression of a YFP fusion to a chimeric FtsZ in which the first 323 residues from *B. subtilis* (the core) were fused to residues 325–383 of *E. coli* (the linker, CTT, and CTV) (see Fig. 5A in Ref. 55). Intriguingly, in their study, Osawa and Erickson (55) were able to obtain second site suppressor mutations in the *E. coli* chromosome that permitted growth of *E. coli* cells expressing the *B. subtilis* chimera protein as its only source of FtsZ. Coupled with the localization data, this finding would support the view that an unidentified FtsZ-interacting protein may titrate ectopic FtsZ away from the site of division. However, this is only speculative because the suppressor mutations isolated in the original paper were never identified at the molecular level.

Role for FtsZ C Terminus in Mediating Lateral Interactions between FtsZ Protofilaments—Based on our findings, we propose a model in which the C terminus of FtsZ plays a central role in mediating interactions between FtsZ protofilaments. Specifically, we envision the FtsZ subunit as a “bucket truck” or “cherry picker” in which the linker serves a function analogous to the boom and the CTT serves a function analogous to the bucket. During FtsZ assembly, the flexible linker would provide the CTT access to subunits on adjacent protofilaments. Interactions between the CTV (and alternatively modulatory proteins bound to the CTV) and the core of adjacent subunits would then function to either promote or inhibit lateral interactions, stabilizing or inhibiting FtsZ assembly as appropriate.

This model is particularly appealing with regard to our understanding of the activity of various FtsZ modulatory proteins. For example, a bundling protein, such as ZipA from *E. coli*, would use the CTT as the equivalent of the bucket on a “cherry picker,” enhancing lateral interactions either through charge shielding or through direct interactions between ZipA and monomers on adjacent protofilaments. Conversely, an inhibitor, such as EzrA from *B. subtilis*, could use its interactions with the CTT terminus to disrupt interaction between the CTV and the core. In the case of EzrA, such an activity would be consistent with both the high degree of bundling observed for *B. subtilis* FtsZ *in vitro* and data suggesting that EzrA is unable to inhibit assembly of *B. subtilis* FtsZ missing 17 C-terminal residues (23).

In summary, we have defined a new role for the FtsZ C terminus that complements its previously identified function as an interaction site for modulatory proteins. Studies of the *in vitro* assembly properties of FtsZs from various species suggest that some (e.g. *B. subtilis* and *Mycobacterium tuberculosis*) (42, 56) bundle to a significantly greater degree than others (e.g. *E. coli* and *C. crescentus*) (3, 57). It will be exciting to determine the impact of the CTV from various species of FtsZ on assembly. For example, *S. aureus* FtsZ, with the highly positively charged CTV sequence NREERRSRRTTRR, would be expected to display a high degree of bundling. Conversely, species of *Actinobacteria* without CTV sequences (Fig. 1B) would be expected to be poor

The C Terminus of FtsZ Mediates Lateral Interactions

bundlers. Interestingly, the two extreme C-terminal arginines of *M. tuberculosis* FtsZ have been shown to be required for assembly *in vitro* (58). It will also be attractive to identify the conserved residues on the FtsZ core involved in stabilizing lateral interactions with the CTT. Finally, this work also highlights the need to characterize the role of the poorly conserved linker in modulating FtsZ assembly dynamics.

Acknowledgments—We thank Bill Margolin for the generous gift of antisera against *E. coli* FtsZ. We also thank Wandy Beatty for assistance with electron microscopy. We are indebted to Laura Romberg, Daniel Haeusser, and Corey Westfall for valuable comments on the manuscript and to members of the Levin laboratory for technical advice, lively discussions, and support.

REFERENCES

1. Harry, E., Monahan, L., and Thompson, L. (2006) Bacterial cell division. The mechanism and its precision. *Int. Rev. Cytol.* **253**, 27–94
2. Anderson, D. E., Gueiros-Filho, F. J., and Erickson, H. P. (2004) Assembly dynamics of FtsZ rings in *Bacillus subtilis* and *Escherichia coli* and effects of FtsZ-regulating proteins. *J. Bacteriol.* **186**, 5775–5781
3. Erickson, H. P., Anderson, D. E., and Osawa, M. (2010) FtsZ in bacterial cytokinesis. Cytoskeleton and force generator all in one. *Microbiol. Mol. Biol. Rev.* **74**, 504–528
4. Mukherjee, A., and Lutkenhaus, J. (1994) Guanine nucleotide-dependent assembly of FtsZ into filaments. *J. Bacteriol.* **176**, 2754–2758
5. Mukherjee, A., and Lutkenhaus, J. (1999) Analysis of FtsZ assembly by light scattering and determination of the role of divalent metal cations. *J. Bacteriol.* **181**, 823–832
6. Gueiros-Filho, F. J., and Losick, R. (2002) A widely conserved bacterial cell division protein that promotes assembly of the tubulin-like protein FtsZ. *Genes Dev.* **16**, 2544–2556
7. Popp, D., Iwasa, M., Narita, A., Erickson, H. P., and Maéda, Y. (2009) FtsZ condensates. An *in vitro* electron microscopy study. *Biopolymers* **91**, 340–350
8. Gündodu, M. E., Kawai, Y., Pavlendova, N., Ogasawara, N., Errington, J., Scheffers, D. J., and Hamoen, L. W. (2011) Large ring polymers align FtsZ polymers for normal septum formation. *EMBO J.* **30**, 617–626
9. Li, Z., Trimble, M. J., Brun, Y. V., and Jensen, G. J. (2007) The structure of FtsZ filaments *in vivo* suggests a force-generating role in cell division. *EMBO J.* **26**, 4694–4708
10. Fu, G., Huang, T., Buss, J., Coltharp, C., Hensel, Z., and Xiao, J. (2010) *In vivo* structure of the *E. coli* FtsZ-ring revealed by photoactivated localization microscopy (PALM). *PLoS One* **5**, e12682
11. Adams, D. W., and Errington, J. (2009) Bacterial cell division. Assembly, maintenance, and disassembly of the Z ring. *Nat. Rev. Microbiol.* **7**, 642–653
12. Löwe, J., and Amos, L. A. (1998) Crystal structure of the bacterial cell division protein FtsZ. *Nature* **391**, 203–206
13. Vaughan, S., Wickstead, B., Gull, K., and Addinall, S. G. (2004) Molecular evolution of FtsZ protein sequences encoded within the genomes of archaea, bacteria, and eukaryota. *J. Mol. Evol.* **58**, 19–29
14. Margolin, W. (2005) FtsZ and the division of prokaryotic cells and organelles. *Nat. Rev. Mol. Cell Biol.* **6**, 862–871
15. Lu, C., Stricker, J., and Erickson, H. P. (2001) Site-specific mutations of FtsZ. Effects on GTPase and *in vitro* assembly. *BMC Microbiol.* **1**, 7
16. Koppelman, C. M., Aarsman, M. E., Postmus, J., Pas, E., Muijsers, A. O., Scheffers, D. J., Nanninga, N., and den Blaauwen, T. (2004) R174 of *Escherichia coli* FtsZ is involved in membrane interaction and protofilament bundling and is essential for cell division. *Mol. Microbiol.* **51**, 645–657
17. Redick, S. D., Stricker, J., Briscoe, G., and Erickson, H. P. (2005) Mutants of FtsZ targeting the protofilament interface. Effects on cell division and GTPase activity. *J. Bacteriol.* **187**, 2727–2736
18. Ma, X., and Margolin, W. (1999) Genetic and functional analyses of the conserved C-terminal core domain of *Escherichia coli* FtsZ. *J. Bacteriol.* **181**, 7531–7544
19. Mosyak, L., Zhang, Y., Glasfeld, E., Haney, S., Stahl, M., Seehra, J., and Somers, W. S. (2000) The bacterial cell division protein ZipA and its interaction with an FtsZ fragment revealed by x-ray crystallography. *EMBO J.* **19**, 3179–3191
20. Haney, S. A., Glasfeld, E., Hale, C., Keeney, D., He, Z., and de Boer, P. (2001) Genetic analysis of the *Escherichia coli* FtsZ-ZipA interaction in the yeast two-hybrid system. Characterization of FtsZ residues essential for the interactions with ZipA and with FtsA. *J. Biol. Chem.* **276**, 11980–11987
21. Din, N., Quardokus, E. M., Sackett, M. J., and Brun, Y. V. (1998) Dominant C-terminal deletions of FtsZ that affect its ability to localize in *Caulobacter* and its interaction with FtsA. *Mol. Microbiol.* **27**, 1051–1063
22. Shen, B., and Lutkenhaus, J. (2009) The conserved C-terminal tail of FtsZ is required for the septal localization and division inhibitory activity of MinC/MinD. *Mol. Microbiol.* **72**, 410–424
23. Singh, J. K., Makde, R. D., Kumar, V., and Panda, D. (2007) Structural basis for ligand binding and specificity in adrenergic receptors. Implications for GPCR-targeted drug discovery. *Biochemistry* **46**, 11013–11022
24. Perego, M., Spiegelman, G. B., and Hoch, J. A. (1988) Structure of the gene for the transition state regulator, *abrB*. Regulator synthesis is controlled by the spo0A sporulation gene in *Bacillus subtilis*. *Mol. Microbiol.* **2**, 689–699
25. Harwood, C. R., and Cutting, S. M. (1990) *Molecular Biological Methods for Bacillus*, John Wiley & Sons, Inc., New York
26. Sambrook, J., and Russell, D. W. (2001) *Molecular Cloning: A Laboratory Manual*, 3rd Ed., Cold Spring Harbor Laboratory, Cold Spring Harbor, NY
27. Ireton, K., Rudner, D. Z., Siranosian, K. J., and Grossman, A. D. (1993) Integration of multiple developmental signals in *Bacillus subtilis* through the Spo0A transcription factor. *Genes Dev.* **7**, 283–294
28. Wang, X., and Lutkenhaus, J. (1993) The FtsZ protein of *Bacillus subtilis* is localized at the division site and has GTPase activity that is dependent upon FtsZ concentration. *Mol. Microbiol.* **9**, 435–442
29. LeDeaux, J. R., and Grossman, A. D. (1995) Isolation and characterization of *kinC*, a gene that encodes a sensor kinase homologous to the sporulation sensor kinases KinA and KinB in *Bacillus subtilis*. *J. Bacteriol.* **177**, 166–175
30. Weart, R. B., and Levin, P. A. (2003) Growth rate-dependent regulation of medial FtsZ ring formation. *J. Bacteriol.* **185**, 2826–2834
31. Haeusser, D. P., Garza, A. C., Buscher, A. Z., and Levin, P. A. (2007) The division inhibitor EzrA contains a seven-residue patch required for maintaining the dynamic nature of the medial FtsZ ring. *J. Bacteriol.* **189**, 9001–9010
32. Levin, P. A., and Losick, R. (1996) Transcription factor Spo0A switches the localization of the cell division protein FtsZ from a medial to a bipolar pattern in *Bacillus subtilis*. *Genes Dev.* **10**, 478–488
33. Weart, R. B., Lee, A. H., Chien, A. C., Haeusser, D. P., Hill, N. S., and Levin, P. A. (2007) A metabolic sensor governing cell size in bacteria. *Cell* **130**, 335–347
34. Miroux, B., and Walker, J. E. (1996) Overproduction of proteins in *Escherichia coli*. Mutant hosts that allow synthesis of some membrane proteins and globular proteins at high levels. *J. Mol. Biol.* **260**, 289–298
35. Romberg, L., Simon, M., and Erickson, H. P. (2001) Polymerization of FtsZ, a bacterial homolog of tubulin. Is assembly cooperative? *J. Biol. Chem.* **276**, 11743–11753
36. Ingerman, E., and Nunnari, J. (2005) A continuous, regenerative coupled GTPase assay for dynamin-related proteins. *Methods Enzymol.* **404**, 611–619
37. Haeusser, D. P., Schwartz, R. L., Smith, A. M., Oates, M. E., and Levin, P. A. (2004) EzrA prevents aberrant cell division by modulating assembly of the cytoskeletal protein FtsZ. *Mol. Microbiol.* **52**, 801–814
38. Mukherjee, A., and Lutkenhaus, J. (1998) Dynamic assembly of FtsZ regulated by GTP hydrolysis. *EMBO J.* **17**, 462–469
39. Pacheco-Gómez, R., Roper, D. I., Dafforn, T. R., and Rodger, A. (2011) The pH dependence of polymerization and bundling by the essential bacterial cytoskeletal protein FtsZ. *PLoS One* **6**, e19369
40. Romberg, L., and Levin, P. A. (2003) Assembly dynamics of the bacterial

- cell division protein FTSZ. Poised at the edge of stability. *Annu. Rev. Microbiol.* **57**, 125–154
41. Froschauer, E. M., Kolisek, M., Dieterich, F., Schweigel, M., and Schweyen, R. J. (2004) Fluorescence measurements of free $[Mg^{2+}]$ by use of mag-fura 2 in *Salmonella enterica*. *FEMS Microbiol. Lett.* **237**, 49–55
 42. Monahan, L. G., Robinson, A., and Harry, E. J. (2009) Lateral FtsZ association and the assembly of the cytokinetic Z ring in bacteria. *Mol. Microbiol.* **74**, 1004–1017
 43. de Oliveira, I. F., de Sousa Borges, A., Kooij, V., Bartosiak-Jentys, J., Luirink, J., and Scheffers, D. J. (2010) Characterization of ftsZ mutations that render *Bacillus subtilis* resistant to MinC. *PLoS One* **5**, e12048
 44. Yu, X. C., and Margolin, W. (1997) Ca^{2+} -mediated GTP-dependent dynamic assembly of bacterial cell division protein FtsZ into asters and polymer networks *in vitro*. *EMBO J.* **16**, 5455–5463
 45. Low, H. H., Moncrieffe, M. C., and Löwe, J. (2004) The crystal structure of ZapA and its modulation of FtsZ polymerization. *J. Mol. Biol.* **341**, 839–852
 46. Lan, G., Dajkovic, A., Wirtz, D., and Sun, S. X. (2008) Polymerization and bundling kinetics of FtsZ filaments. *Biophys. J.* **95**, 4045–4056
 47. Yan, K., Pearce, K. H., and Payne, D. J. (2000) A conserved residue at the extreme C terminus of FtsZ is critical for the FtsA-FtsZ interaction in *Staphylococcus aureus*. *Biochem. Biophys. Res. Commun.* **270**, 387–392
 48. Jensen, S. O., Thompson, L. S., and Harry, E. J. (2005) Cell division in *Bacillus subtilis*. FtsZ and FtsA association is Z-ring-independent, and FtsA is required for efficient midcell Z-ring assembly. *J. Bacteriol.* **187**, 6536–6544
 49. Ishikawa, S., Kawai, Y., Hiramatsu, K., Kuwano, M., and Ogasawara, N. (2006) A new FtsZ-interacting protein, YlmF, complements the activity of FtsA during progression of cell division in *Bacillus subtilis*. *Mol. Microbiol.* **60**, 1364–1380
 50. RayChaudhuri, D., and Park, J. T. (1994) A point mutation converts *Escherichia coli* FtsZ septation GTPase to an ATPase. *J. Biol. Chem.* **269**, 22941–22944
 51. Bi, E., and Lutkenhaus, J. (1992) Isolation and characterization of ftsZ alleles that affect septal morphology. *J. Bacteriol.* **174**, 5414–5423
 52. Dai, K., Mukherjee, A., Xu, Y., and Lutkenhaus, J. (1994) Mutations in ftsZ that confer resistance to SulA affect the interaction of FtsZ with GTP. *J. Bacteriol.* **176**, 130–136
 53. RayChaudhuri, D. (1999) ZipA is a MAP-Tau homolog and is essential for structural integrity of the cytokinetic FtsZ ring during bacterial cell division. *EMBO J.* **18**, 2372–2383
 54. Beall, B., Lowe, M., and Lutkenhaus, J. (1988) Cloning and characterization of *Bacillus subtilis* homologs of *Escherichia coli* cell division genes ftsZ and ftsA. *J. Bacteriol.* **170**, 4855–4864
 55. Osawa, M., and Erickson, H. P. (2006) FtsZ from divergent foreign bacteria can function for cell division in *Escherichia coli*. *J. Bacteriol.* **188**, 7132–7140
 56. Chen, Y., Anderson, D. E., Rajagopalan, M., and Erickson, H. P. (2007) Assembly dynamics of *Mycobacterium tuberculosis* FtsZ. *J. Biol. Chem.* **282**, 27736–27743
 57. Goley, E. D., Dye, N. A., Werner, J. N., Gitai, Z., and Shapiro, L. (2010) Imaging-based identification of a critical regulator of FtsZ protofilament curvature in *Caulobacter*. *Mol. Cell* **39**, 975–987
 58. Gupta, P., Rajeswari, H., Arumugam, M., Mishra, S., Bhagavat, R., Anand, P., Chandra, N., Srinivasan, R., Indi, S., and Ajitkumar, P. (2010) Mycobacterium tuberculosis FtsZ requires at least one arginine residue at the C-terminal end for polymerization *in vitro*. *Acta Biochim. Biophys. Sin.* **42**, 58–69
 59. Raymond, A., Lovell, S., Lorimer, D., Walchli, J., Mixon, M., Wallace, E., Thompkins, K., Archer, K., Burgin, A., and Stewart, L. (2009) Combined protein construct and synthetic gene engineering for heterologous protein expression and crystallization using Gene Composer. *BMC Biotechnol.* **9**, 37